PHILOSOPHICAL TRANSACTIONS B

royalsocietypublishing.org/journal/rstb

Research

Cite this article: Laird MF, Iriarte-Diaz J, Byron CD, Granatosky MC, Taylor AB, Ross CF. 2023 Gape drives regional variation in temporalis architectural dynamics in tufted capuchins. *Phil. Trans. R. Soc. B* **378**: 20220550.
https://doi.org/10.1098/rstb.2022.0550

Received: 27 January 2023
Accepted: 10 June 2023

One contribution of 18 to a theme issue 'Food processing and nutritional assimilation in animals'.

Subject Areas:
biomechanics, behaviour

Keywords:
muscle, feeding, primate

Author for correspondence:
Myra F. Laird
e-mail: mflaird@upenn.edu

Electronic supplementary material is available online at https://doi.org/10.6084/m9.figshare.c.6836738.

THE ROYAL SOCIETY PUBLISHING

Gape drives regional variation in temporalis architectural dynamics in tufted capuchins

Myra F. Laird[1], Jose Iriarte-Diaz[2], Craig D. Byron[3], Michael C. Granatosky[4], Andrea B. Taylor[5] and Callum F. Ross[6]

[1]Department of Basic and Translational Sciences, University of Pennsylvania, Levy 443, 4010 Locust Street, Philadelphia, PA 19104, USA
[2]Department of Biology, University of the South, Sewanee, TN 37383-1000, USA
[3]Department of Biology, Mercer University, Macon, GA 312014, USA
[4]Department of Anatomy, New York Institute of Technology, Old Westbury, NY 11545, USA
[5]Department of Foundational Biomedical Sciences, Touro University, Vallejo, CA 94592, USA
[6]Department of Organismal Biology and Anatomy, University of Chicago, Chicago, IL 60637, USA

MFL, 0000-0002-8636-0407; MCG, 0000-0002-6465-5386; CFR, 0000-0001-7764-761X

Dynamic changes in jaw movements and bite forces depend on muscle architectural and neural factors that have rarely been compared within the same muscle. Here we investigate how regional muscle architecture dynamics—fascicle rotation, shortening, lengthening and architectural gear ratio (AGR)—vary during chewing across a functionally heterogeneous muscle. We evaluate whether timing in architecture dynamics relates to gape, food material properties and/or muscle activation. We also examine whether static estimates of temporalis fibre architecture track variation in dynamic architecture. Fascicle-level architecture dynamics were measured in three regions of the superficial temporalis of three adult tufted capuchins (*Sapajus apella*) using biplanar videoradiography and the XROMM workflow. Architecture dynamics data were paired with regional fine-wire electromyography data from four adult tufted capuchins. Gape accounted for most architectural change across the temporalis, but architectural dynamics varied between regions. Mechanically challenging foods were associated with lower AGRs in the anterior region. The timing of most dynamic architectural changes did not vary between regions and differed from regional variation in static architecture. Collectively these findings suggest that, when modelling temporalis muscle force production in extant and fossil primates, it is important to account for the effects of gape, regionalization and food material properties.

This article is part of the theme issue 'Food processing and nutritional assimilation in animals'.

1. Introduction

The jaw muscles produce the forces necessary for moving the jaw and generating bite force. Thus, jaw muscle mechanics are key to understanding form–function relationships in the feeding system. Maximum force-generating capacity of the jaw muscles can be estimated using muscle mass, fibre length and pinnation angle to calculate their physiological cross-sectional areas (PCSAs) [1–4]. Fibre lengths of the chewing muscles, and thus architectural variables that depend on estimates of fibre length such as PCSA, are influenced by joint posture (e.g. [5,6]). Likewise, estimates of the force-generating capacity of the chewing muscles are influenced by the composition and distribution of fibre types (e.g. [7,8]). How this muscle force is converted (amplified and transmitted) into jaw movement and bite and joint reaction forces is a function of their moment arms. Muscle moment arms are impacted by the relative positions of the jaw joint, coronoid process, mandibular angle and tooth row. The static configurations of these

features have been extensively studied (e.g. [9–15]), but dynamic changes in muscle architecture during feeding have only recently been investigated [16].

Iriarte-Diaz *et al*. used three-dimensional (3D) jaw kinematics to quantify *in vivo* dynamics of whole muscle lengths (from origin to insertion) and moment arms of the superficial anterior (SAT), middle (SMT) and posterior (SPT) temporalis relative to the axis of rotation through the ramus. They compared these results with the hypothetical dynamics if the axis of rotation was through the temporomandibular joints (TMJs) [17]. They found that, although the actual location of the axis of rotation of the mandible—through the ramus—increases stretch in the SAT, SMT and SPT more than if the axis passed through the TMJs, it decreases the differences in muscle strain between SAT and SPT. They concluded that: 'anterior and posterior fibres of the temporalis can operate at similar points on the length–tension curve through large parts of the gape cycle', potentially allowing the temporalis to generate consistent forces across the whole muscle [17, p. 117]. These findings support the hypothesis that the temporalis functions to generate vertically oriented bite force across a wide range of gapes and behaviours [18–20].

However, although whole muscle length dynamics of the SAT, SMT and SPT can be approximated using vectors from origin to insertion, they do not capture dynamics of fascicles that are not oriented along this line, in either sagittal or coronal planes. These dynamics are necessary to assess the impact of whole muscle length dynamics on force production capacity of the jaw muscles. One way to quantify these effects is with architectural gear ratios (AGRs), the ratio of whole muscle strain or velocity to that of individual fascicles [16,21–25]. High AGRs are associated with greater fascicle rotation, resulting in larger changes in fascicle angle, higher muscle shortening velocity relative to fascicle shortening, and hence faster movements. By contrast, low AGRs are characterized by less fascicle rotation, reduced changes in fascicle angle, and similar amounts of muscle and fascicle shortening, and thus favour force production [21].

We recently used fluoromicrometry—biplanar videoradiography and the X-ray reconstruction of moving morphology (XROMM) workflow [26]—to measure muscle architecture dynamics, i.e. rotation, shortening, lengthening and gearing (AGR) of muscle fascicles in the SAT of capuchin monkeys [16]. Our data showed that most of the architectural changes in the capuchin SAT during chewing are driven by changes in gape and that SAT fascicles rotated much more in sagittal (10–30°) than in coronal planes (less than 5°) [16]. We also found that AGRs in the SAT were lower when the animals chewed on more mechanically resistant foods than when chewing on less resistant foods, suggesting a role for muscle architecture dynamics in modulating muscle force in response to changing food material properties [16]. This study raises several questions, the answers to which have important implications for understanding temporalis muscle mechanics during feeding and our ability to model temporalis force production in extant and extinct taxa.

First, are muscle architecture dynamics in the SMT and SPT driven primarily by gape, as is the case in SAT, and are the gape–architecture relationships similar across muscle regions? The dynamics of whole muscle lengths certainly vary across different parts of the capuchin temporalis during chewing [17], raising the question of whether this is also true of muscle fascicle lengths and orientations.

Second, are the food material property (FMP) effects that we documented in the SAT also seen in the SMT and SPT? Diversity in the effects of FMPs on muscle architecture dynamics would have significant implications for our understanding of feeding behaviour- and diet-related adaptations in primate jaw elevator muscles.

Third, what role might muscle activation patterns play in modulating muscle architecture dynamics in different parts of the temporalis? The evidence surrounding this question is mixed, with some studies suggesting muscle AGR is largely independent of central nervous system (CNS) activity: shape changes occur in isolated muscle preparations independent of any CNS afferents or efferents [21], architectural shape changes are not correlated with muscle activation in arm muscles [27], and architecture dynamics can drive regional differences in a muscle's force output under conditions of constant neural stimulation [28]. By contrast, there is a strong relationship between pinnation angle and muscle activation in human erector spinae muscles [29] and variable recruitment can shift regional architectural patterns in rat gastrocnemius [30]. Moreover, the CNS dynamically changes the frequency of recruitment and activation of muscle motor units [31–39]. How muscle architecture dynamics and CNS-driven motor unit recruitment interact to achieve task-specific jaw movements and bite force production during feeding is fundamental for understanding form–function relationships in the feeding system [28,30,40–46]. In particular, we are interested in whether temporalis muscle activation patterns modulate temporalis muscle architecture dynamics independent of gape, or whether temporalis architecture dynamics are driven primarily by changes in jaw gape. Support for the latter would simplify modelling of temporalis force production during feeding in living and extinct primates. Here, we present data on muscle activation patterns across the temporalis and on the relative timing of muscle architecture dynamics in capuchins.

Fourth, what are the implications of muscle architecture dynamics for estimates of jaw-muscle force based on static measurements of muscle architecture? Jaw kinematics during feeding dynamically alter the moment arms, force–length and force–velocity relations of the jaw muscles [47–53]. Yet studies estimating jaw-muscle force and excursion across a wide range of vertebrates—from turtles, snakes and bats to human and nonhuman primates—have been based predominantly on static measurements of muscle architecture [54–63]. Moreover, static estimates of jaw-muscle force in extant taxa have been used to model and estimate bite force in extinct taxa (e.g. [64–66]. Here, we use this opportunity to evaluate how closely patterns of variation in static architecture measures (fibre length, pinnation angle) across the temporalis track patterns of variation in architecture dynamics across the temporalis muscle.

The temporalis muscle is ideal for *in vivo* feeding studies of muscle architecture dynamics. The temporalis is a fan-shaped muscle divided by a central tendon into deep and superficial compartments. The superficial compartment can be subdivided into anterior, middle and posterior regions based on vector orientation and muscle recruitment patterns [67]. The primate SAT is primarily associated with jaw elevation, whereas the SPT is active during jaw elevation and retraction. The SAT in particular is recruited during a

wide range of feeding behaviours [18,68–70], but in baboons (at least) is especially active during chewing on hard foods [67,71]. Here, we examine variation in muscle architecture dynamics in the anterior, middle and posterior superficial temporalis at sub-maximal activation levels during natural feeding in tufted capuchin monkeys (*Sapajus apella*). Specifically, we address whether muscle architecture dynamics vary along the temporalis, and the extent to which these architecture dynamics vary with gape, FMPs and static architecture. We also address whether the timing of architecture dynamics across the temporalis is predicted by timing of muscle activity. We test four hypotheses:

(a) Hypothesis 1

Muscle architecture dynamics in the SAT, SMT and SPT vary with gape. Modelling of whole muscle–tendon unit strain based on *in vivo* measures of jaw kinematics reveals that strain in anterior, middle and posterior temporalis muscle regions increases with gape, and that at wide jaw gapes the anterior temporalis undergoes more stretch than middle and posterior muscle regions [17]. Our previous work showed that change in gape is also the primary driver of the majority of variation in SAT architecture dynamics (e.g. fascicle and whole muscle lengths, instantaneous fascicle and muscle shortening, AGR) [16]. However, we did not measure the impact of gape on SMT and SPT architecture dynamics. Here, we predict that, as with the SAT, architecture dynamics of the SMT and SPT vary with gape, but that the magnitude of this effect is greatest in the SAT and decreases from anterior to posterior across the muscle [17]. Our null hypothesis is that the effects of gape on variation in architecture dynamics are similar for all three regions of the temporalis.

(b) Hypothesis 2

Unlike the SAT, muscle architecture dynamics in the SMT and SPT do not vary with FMPs. In our previous work, we found that muscle architecture dynamics in the SAT varied such that mechanically challenging foods were associated with lower AGRs [16]. As the SAT is expected to undergo the highest amounts of variation in architecture dynamics (Hypothesis 1), we predict that AGRs in the SMT and SPT will vary less with foods of different material properties than in the SAT. Our null hypothesis is that FMP-associated muscle architecture dynamics in the SMT and SPT will be similar to those in the SAT.

(c) Hypothesis 3

The timing of muscle architecture dynamics varies between SAT, SMT and SPT. Electromyographic (EMG) data in thick-tailed galagos, ring-tailed lemurs, owl monkeys, macaques and baboons suggest that the SPT is activated before the SAT and SMT on the working side and after the SAT on the balancing side during chewing [18–20,67,72]. If muscle architecture dynamics are driven primarily by muscle activity patterns rather than gape, then changes in muscle architecture dynamics in the SPT will precede those in the SAT on the working side and follow them on the balancing side. Our null hypothesis is that the timing of muscle architecture dynamics does not vary between regions.

(d) Hypothesis 4

Patterns of variation across the SAT, SMT and SPT differ between dynamic and static architecture variables. In tufted capuchins, we have observed minimal variation in static estimates of fibre length and pinnation angle measured at or near occlusion across the SAT, SMT and SPT (i.e. less than 1 mm difference in average fibre lengths and less than 1° of difference in average pinnation angle across the three regions; (A. B. Taylor 2023, unpublished data). However, whole muscle stretch is expected to be larger in the SAT than the SMT and SPT because of the positioning of the SAT to the jaw joint [6,17,48]. Taken together, these data lead us to predict that patterns of static architectural variables measured at or near occlusion differ from patterns of dynamic architecture variables measured during the slow-close phase of the gape cycle. Our null hypothesis is that static architecture patterns are similar to patterns of muscle architecture dynamics across the temporalis.

2. Material and methods

(a) Subjects

Data were collected from a total of seven tufted capuchins (*Sapajus apella*)—dynamic muscle architecture data from three adult females, and EMG data from three adult males and one adult female. All animals were housed at the University of Chicago's Animal Resources Center. During data recording, body masses ranged between 2.1 and 2.4 kg for the females and between 2.8 and 4.7 kg for the males. All experiments were approved by the University of Chicago IACUC under Animal Care and Use Protocols 72430 and 72382. Static architectural measurements for the temporalis muscle were obtained from the same three males and one female used in the EMG experiments in addition to two other females that were not part of the *in vivo* data collection. It was not possible to collect static muscle architecture, EMG and dynamic muscle architecture data all from the same animals. Consequently, our static architecture and EMG data are not from the same animals as our muscle architecture dynamics data.

(b) Dynamic muscle architecture

Dynamic muscle architecture data were collected using the XROMM workflow [73] and methods described in [16]. Four 1 mm tantalum spheres (Bal-Tec, Los Angeles, CA, USA) were implanted into both the cranium and mandible of each animal, and two laser-drilled tantalum beads were sutured (using 6/0 Vicryl) into a single fascicle in each of the anterior, middle and posterior regions of the right temporalis. In each region, the muscle was divided parallel to the fascicles to expose the central myotendinous junction, and a single fascicle was traced from the central myotendinous junction to its superficial termination. A drilled tantalum sphere was sutured to either end of the fascicle. Superior to each marked fascicle, in the same coronal plane as the sphere at the central myotendinous junction, an additional tantalum sphere was placed at the superior termination of the temporalis muscle (figure 1). The anterior fascicle markers were placed at approximately the point of greatest postorbital constriction. The posterior termination of the temporalis muscle was palpated, and the posterior fascicle markers were inserted approximately 10 mm anterior to the muscle's posterior termination. The middle temporalis markers were placed halfway between the anterior and posterior markers. While all markers were placed in roughly homologous locations, the exact placement of the markers differed between subjects (figure 1). The temporalis muscle was sutured following marker insertion, and

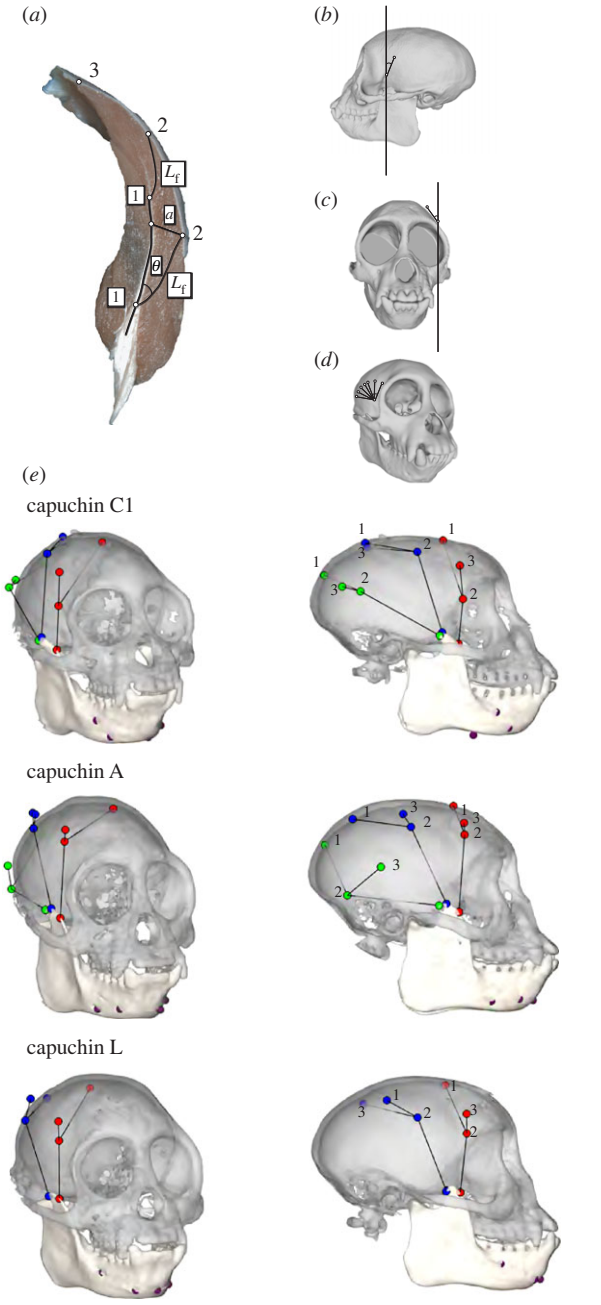

Figure 1. (*a*) A coronal section of a capuchin right temporalis in anterior view. Static muscle fibre length (L_f) and pinnation angle (θ) were measured between the central myotendinous junction and the fibre superficial termination. For dynamic muscle architecture, tantalum beads were sutured to the central myotendinous junction of a single fascicle (1), the superficial termination of that fascicle (2), and at the temporal fascia line directly superior to beads 1 and 2 (3). Fascicle angles were measured by passing planes between makers 1 and 3 in a coronal plane for (*b*) sagittal fascicle angle, and in the sagittal plane for (*c*) coronal fascicle angle. (*d*) Three-dimensional angle was measured as the change in angulation between markers 1–3 during a gape cycle. (*e*) Locations of the fascicle markers in the superficial anterior temporalis (SAT, in red), superficial middle temporalis (SMT, in blue) and superficial posterior temporalis (SPT, in green) for capuchin A, C1 and L.

an additional suture was used to close the incision in the overlying temporalis fascia in order to reduce the effect of aponeurosis modification [74]. The animals recovered for two weeks prior to recording.

During data recording each animal was fed five foods: popcorn seeds, whole roasted cashews (without shells), red grapes (cut in half), miniature marshmallows and 15 mm diameter cubes of apple pulp (without skin) (table 1). These foods ranged in food material properties (FMPs), namely toughness ($J\,m^{-2}$), the work needed to propagate a crack through an object, and elastic modulus (MPa), the ratio of stress to strain within the elastic region: from popcorn seeds ($2978.82 \pm 678.34\,J\,m^{-2}$; 325.4 ± 218.83 MPa, respectively) to apple pulp ($56.97 \pm 17.76\,Jm^{-2}$; 3.41 ± 0.10 MPa, respectively) [16,75]. Toughness and elastic modulus values for all foods are available in [16]. For the purposes of comparison, popcorn seeds and cashews were grouped as more mechanically challenging foods, and marshmallows, grapes and cubes of apple pulp were grouped as less mechanically challenging.

All chewing trials were recorded using biplanar videoradiography (90 kVp, 100 mA) at 150 frames per second (fps) using ProCapture software (Xcitex). Standardized grids and a cube with known geometry were used to calibrate the 3D recording space. Tantalum spheres were tracked using XMALab v1.5.5 (bitbucket.org/xromm/xmalab), resulting in *xyz* coordinates for each tantalum sphere. Fascicle length was measured as the distance between the coordinates of the two fascicle markers and was normalized to minimum fascicle distance (between markers1 and 2 in figure 1*a*). Muscle length was the distance from the coronoid process to the superior muscle attachment of each muscle region, and instantaneous fascicle and muscle velocities were the temporal derivatives of fascicle and muscle distance respectively. Architectural gear ratio (AGR) was measured as the ratio of whole muscle to fascicle velocity. Fascicle angles were defined in three ways: fascicle angle, a 3D measure of the angle between the fascicle and the central myotendinous junction; sagittal fascicle angle, measured within sagittal planes; and coronal fascicle angle, measured in coronal planes. All fascicle angles were normalized to their maximum values, meaning that change in fascicle angle was compared across jaw closing. These fascicle angles capture the rotation of the fascicle as it relates to AGR. These coordinate data were filtered using a low-pass Butterworth filter with 30 Hz cut-off frequency in the R package 'signal' [76]. Spatial precision of these marker techniques is estimated to be 0.1–0.2 mm [77]. Mandibular movements at the condyle were constrained by adding an additional virtual marker located midway between the left and right temporal fossae to reduce effects of digitizing error on mandibular displacement measures. The animals were unrestrained within the recording chamber, and all gape cycles with complete recordings were included in the analyses.

Subject-specific computed tomographic (CT) scans were collected using a Vimago Robotic HDC scanner (Epica Medical Innovations), and the scans were processed in Horos v3.3.6 (horosproject.org). The 3D positions of the tantalum beads implanted on the cranium and mandible were extracted from 3D models of the processed CT scans in MeshLab v2020 (meshlab.net). The CT-derived cranial and mandibular landmarks were used as the reference position, with the mandible in centric occlusion. Rigid body kinematics of the mandible were described using the 4×4 homogeneous transformation matrices of the digitized cranial and mandibular markers at different time steps with respect to the reference position, calculated using singular value decomposition methods [78].

(c) Static muscle architecture

We used previously published protocols for obtaining architectural measurements of the temporalis muscle [61,79,80]. Briefly, muscles were harvested en masse from the skull, trimmed of fat and fascia, blotted dry and weighed to the nearest 0.001 g. The muscles were then sectioned along their lengths into anterior, middle and posterior regions based on external fibre orientation, and each region was weighed to the nearest 0.001 g. For each muscle, a maximum of six fibre length (L_f) measurements was taken from each of the proximal and distal regions of the superficial and deep anterior, middle and posterior temporalis, for a

Table 1. Number of chewing cycles analysed for each animal and food type.

dynamic muscle architecture data					
food	**capuchin A**	**capuchin C1**	**capuchin L**	**total no. of gape cycles**	
apple (without skin)	3	3	6	12	
cashew (without shell)	6	3	4	13	
grape	2	14	8	24	
marshmallow	19	7	10	36	
popcorn seeds		4	12	16	
electromyography data					
food	**capuchin C2**	**capuchin Mo**	**capuchin N**	**capuchin Se**	**total no. of gape cycles**
almond	212	48	115	248	375
apple	176				424
apricot	66		13	139	218
banana		147			147
banana chip	11		6	17	
brazil nut	690	87	29	405	1211
cashew			36	387	423
coconut				239	239
craisin		36			36
date			19		19
fruit loop	101			101	
grape		84	90	96	270
hazelnut	378	119	201	89	787
papaya			61		61
peanut		230		56	286
pecan	234	111			345
pineapple		60		60	
raisin				44	44
walnut	611	46	133	254	1044

maximum total of 24 measurements per muscle region and 72 measurements per muscle (figure 1*a*). Measurements from the right and left sides were averaged when possible. A second measure was recorded as the perpendicular distance from the tendon of insertion to the proximal fibre attachment (*a*). Pinnation angle (θ) of each measured fibre was estimated as arcsin a/L_f (figure 1*a*). Only intact, uncut fibres running from tendon attachment to tendon attachment were measured [6].

Raw fibre lengths were normalized to control for variation in jaw posture among individuals at the time of fixation [6]. To accomplish this, *in situ* sarcomere lengths (± 0.01 µm) from the measured fibres were obtained using laser diffraction [81]. Raw L_f then was normalized (NL_f) employing the following equation:

$$NL_f = \frac{L_f L_{so}}{L_s},$$

where NL_f is the normalized fibre length (cm), L_f is the experimentally measured fibre length (mm), L_{so} is the standardized sarcomere length (2.41 µm; [82]) and L_s is the experimentally measured sarcomere length (µm).

Average fibre lengths and pinnation angles were calculated for the anterior, middle and posterior regions and for the entire temporalis muscle. Physiological cross-sectional areas (PCSAs, cm^2) were estimated for each muscle region and for the entire muscle, employing regional and whole muscle masses, respectively, and a muscle-specific density of 1.0564 g cm^{-3} [83]. Regional and whole muscle fibre lengths, pinnation angles and PCSAs were estimated for both raw and normalized data and both were used for data analysis.

$$\text{PCSA } (cm^2) = \text{muscle weight (g)} \times \cos\theta / NL_f \times 1.0564 \text{ (g cm}^{-3}).$$

(d) Electromyography

The EMG data were collected using indwelling bipolar fine-wire electrodes following procedures described in Byron *et al*. [84]. Briefly, the ends of two EMG wires were threaded into a 25-gauge or smaller hypodermic needle, then folded against the needle shaft to create a hook. The needle was then inserted into the temporalis or masseter muscle and carefully removed leaving the wires in place. Wire placement was verified by stimulation, and the incisions closed with 4/0 Vicryl. Wires were placed bilaterally in the superficial masseter and in the SAT, SMT and SPT. Animals were given at least two weeks to recover before beginning data collection.

EMG data were recorded for 6107 gape cycles across 20 foods (table 1) and classified as working or balancing side (ipsilateral

or contralateral to the electrodes) based on jaw kinematics. All data were passed through a band-pass filter (100–2000 Hz), fully rectified, and root-mean-squared (RMS) values were calculated in 42 ms time constant in 2 ms intervals [68,85]. The RMS data were used to find the timing of peak amplitude (in milliseconds) during a gape cycle. To compare across animals, the timing of peak amplitude and 75, 50 and 25% of peak amplitude on either side of the peak were extracted for the working and balancing SAT, SMT and SPT and ordered relative to the working-side superficial masseter (electronic supplementary material, figure S1) [68,85].

(e) Analyses

All analyses were conducted in R v3.6.2 [86] and significance was set at $p < 0.05$ for all tests. Relationships between regional muscle architecture dynamics and gape (Hypothesis 1), regional differences in AGR with FMPs (Hypothesis 2), timing of dynamic architecture measures (Hypothesis 3) and regional differences in static muscle architecture (Hypothesis 4) were tested using linear mixed effects (LME) models fitted by maximum likelihood. These models control for random error introduced by repeated measures, such as multiple gape cycles from the same animal. For the dynamic architecture variables, random factors were nested as gape cycle order within food type within subject, and subject was designated as a random factor in static architecture models.

For Hypothesis 1, LME models between dynamic architecture variables and gape were compared using the R package 'MuMIn' to calculate the marginal R^2 values (R^2_m), quantifying how well the fixed terms fitted the model [87]. LME models of regional differences in AGR values between 'high' and 'low' FMP groups (Hypothesis 2) were tested using analyses of variance (ANOVAs). Differences in the timing of muscle activation were tested using rankings (Hypothesis 3). Working- and balancing-side muscles were assigned ranks based on the timing of their peak activation relative to the superficial masseter. For example, if peak activation of the working-side SPT appeared first relative to the superficial masseter, the working-side SPT received a rank of 1. Similarly, the timing of maximum or minimum dynamic muscle architecture variables was compared between the working and balancing sides. All architectural variables were compared between regions before and after dividing by normalized gape, normalized to the change in distance from minimum gape, to test for timing differences in gape-normalized architectural variables. Differences between the SAT, SMT and SPT in the ranks or locations of minimum or maximum EMG or dynamic architecture variables (Hypothesis 3) and static muscle architecture (Hypothesis 4) were tested using LME models analysed with ANOVA and *post hoc* Tukey comparisons performed in the R package 'multicomp', and the sequential Bonferroni adjustment used to minimize type 1 error [88].

3. Results

(a) Hypothesis 1. Muscle architecture dynamics of the SAT, SMT and SPT vary with gape

During jaw closing, fascicle and muscle lengths in the SAT, SMT and SPT were longest at maximum gape (jaw open) and smallest at minimum gape (jaw closed); 3D, sagittal and coronal angles in most temporalis regions were smallest at maximum gape and largest at minimum gape (figure 2 and table 2; electronic supplementary material, table S1). The SPT 3D angle was largest at maximum gape and decreased to minimum gape. During jaw closing, instantaneous fascicle and muscle shortening velocity increased from maximum gape (when they were zero) until approximately 25% of the gape cycle, around the start of slow close, and then decreased until minimum gape (50% of the gape cycle). Architectural gear ratio (AGR) varied little from maximum gape to minimum gape (figure 2).

The SAT, SMT and SPT fascicle and muscle lengths all significantly positively varied with gape (all $p < 0.01$; electronic supplementary material, table S2). The variation between fascicle length and gape was highest in the SAT (R^2_m SAT = 0.93), and lower in the SMT and SPT (R^2_m SMT = 0.73, R^2_m SPT = 0.71). The SAT, SMT and SPT 3D angles, coronal angles and sagittal angles significantly negatively varied with gape, except for 3D angle of the SPT (all $p < 0.01$; electronic supplementary material, table S2). The variations between 3D angles, coronal angles and gape were higher in the SAT and SPT than the SMT, and the variation between sagittal angle and gape was highest in the SPT (electronic supplementary material, table S2). AGR did not vary with gape (electronic supplementary material, table S2). Fascicle and muscle velocities did not vary with gape because peak velocities occurred during the middle of jaw closing, when the teeth were coming into occlusion.

(b) Hypothesis 2. Unlike in the SAT, AGRs in the SMT and SPT do not vary with FMPs

As reported previously [16], when tufted capuchins chewed on mechanically challenging foods the SAT was associated with significantly lower AGRs than when chewing on less mechanically challenging foods ($p = 0.03$; figure 3; electronic supplementary material, table S3). By contrast, AGRs in the SPT were significantly higher when the animals fed on more mechanically challenging foods ($p = 0.03$). There were no significant differences ($p > 0.05$) in AGRs between foods of differing mechanical properties in the SMT (electronic supplementary material, table S3).

(c) Hypothesis 3. The timing of muscle architecture dynamics varies between SAT, SMT and SPT

As reported in Byron *et al*. [84], the working-side SPT peaks significantly earlier than the balancing-side SMT and SPT, and the working-side SMT and superficial masseter (all $p < 0.05$; electronic supplementary material, figure S1 and table S4) in rank order comparisons. These comparisons also suggest the working-side SAT peaks significantly earlier than the balancing-side SPT, which peaks significantly later than the balancing-side SAT (both $p < 0.05$; electronic supplementary material, table S4). In contrast with the EMG data, the timing of regional changes in dynamic muscle architecture did not show a consistent pattern between the working and balancing sides and before or after normalizing for gape. However, there were significant differences in timing of some muscle architecture variables between regions. On the working side before and after gape correction, there were no differences in fascicle length, but on the balancing side before and after gape correction the maximum SMT fascicle length occurred significantly earlier than in the SAT and SPT ($p < 0.05$; electronic supplementary material, figure S2 and table S5). With a few exceptions, before and after gape correction (3D, sagittal and coronal) working-side angles in the SPT and SMT differed significantly from those in the SAT ($p < 0.05$; electronic supplementary material, figure S2 and table S5), whereas there were few regional differences in these angles on the balancing side. Fascicle

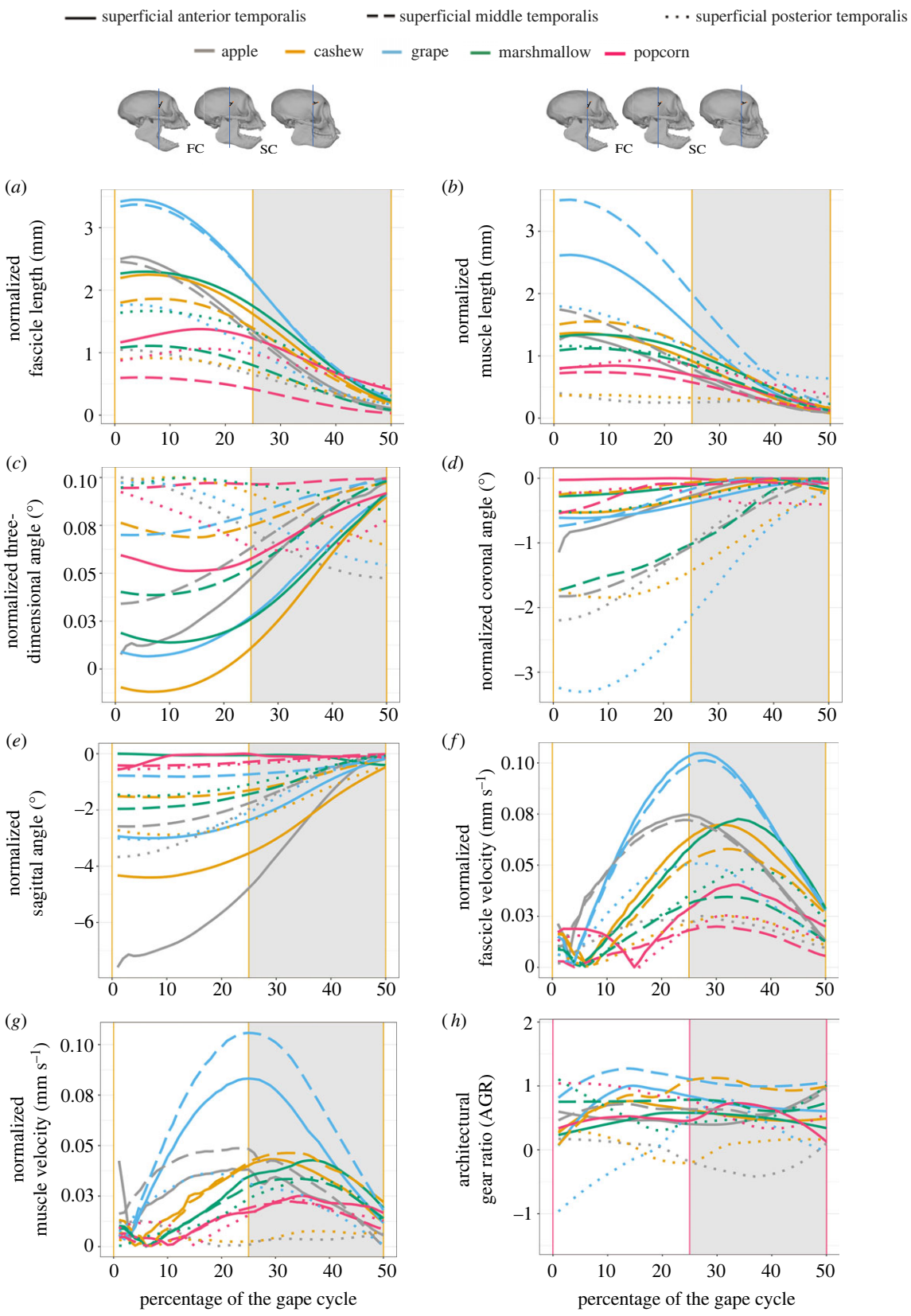

Figure 2. Average gape cycles for each region of the temporalis and each food from the three female capuchins. The full dataset was used in these figures (see also electronic supplementary material, table S1). Compared with the superficial posterior temporalis (SPT), the superficial anterior temporalis (SAT) showed greater and more variable fascicle distance (*a*) and muscle distance (*b*), smaller and more variable 3D angle (*c*) and sagittal angle (*e*), but smaller and less variable coronal angle (*d*). Fascicle velocity (*f*) and muscle velocity (*g*) in the SAT were larger and more variable compared with the SPT, and the SAT had higher architectural gear ratio (*h*) values during jaw closing (0–50% of the gape cycle). Fascicle and muscle distances and 3D, coronal, and sagittal fascicle angles were largest during the fast-close (FC) phase (white background), whereas fascicle and muscle velocities were largest during the FC/SC transition (grey background—slow-close phase). All trends were generated using LOESS fits with a 25% smoothing span.

and muscle velocity and AGR values before and after gape correction showed regional differences, with peak SMT and SPT values generally occurring later than the SAT ($p < 0.05$; electronic supplementary material, figure S2 and table S5), and these measures were consistent between the working and balancing sides.

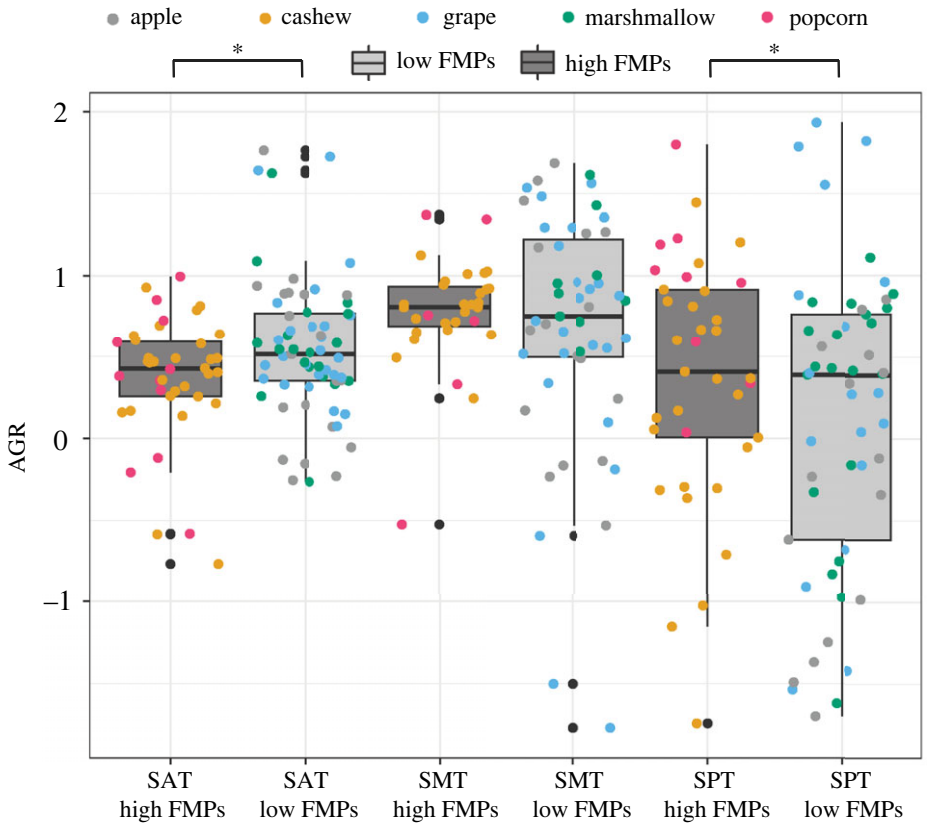

Figure 3. Boxplot comparing architectural gear ratios (AGR) for the superficial anterior (SAT), middle (SMT) and posterior (SPT) temporalis when tufted capuchins fed on high food material property (FMP) items (i.e. popcorn and shelled cashews) and low FMP items (i.e. marshmallow, grapes and cubes of apple pulp). SAT AGRs were lower and SPT AGRs were higher when the animals fed on mechanically challenging foods. SMT AGR values did not differ between foods varying in FMPs (see also electronic supplementary material, table S3). The upper and lower bounds of the boxes correspond with the 25th and 75th percentiles and the whiskers extend 1.5 times the interquartile range in either direction. The median is represented by a horizontal line inside the boxes. Significance ($p < 0.05$) is indicated by one asterisk.

Table 2. Maximum fascicle and muscle lengths and minimum 3D, coronal and sagittal angles (with standard deviations in parentheses) of dynamic muscle architecture variables during jaw closing for the superficial anterior (SAT), middle (SMT) and posterior (SPT) temporalis for each of the three female adult tufted capuchins. Static fibre length and pinnation angle (table 3) are not directly comparable to dynamic fascicle length and angles because of differences in measurement.

capuchin	muscle region	normalized maximum fascicle length (mm)	normalized maximum muscle length (mm)	normalized minimum 3D angle (°)	normalized minimum coronal angle (°)	normalized minimum sagittal angle (°)
A	SAT	1.44 (1.15)	0.87 (0.79)	−0.15 (0.13)	−0.47 (0.46)	−3.93 (2.96)
A	SMT	1.53 (1.24)	1.15 (0.96)	−0.06 (0.06)	−0.72 (0.82)	−1.08 (0.99)
A	SPT	0.53 (0.65)	0.25 (0.41)	−0.05 (0.05)	−1.43 (1.28)	−2.21 (1.73)
C1	SAT	1.99 (1.71)	1.46 (1.59)	−0.07 (0.14)	−0.26 (0.22)	−1.19 (0.87)
C1	SMT	1.83 (1.57)	2.37 (2.09)	−0.01 (0.01)	−1.14 (0.99)	−0.17 (0.12)
C1	SPT	1.44 (1.34)	1.88 (1.74)	−0.12 (0.31)	−1.79 (1.38)	−0.15 (0.12)
L	SAT	1.58 (1.02)	0.87 (0.55)	−0.11 (0.07)	−0.17 (0.23)	−2.84 (2.72)
L	SMT	1.57 (0.97)	1.32 (0.84)	−0.03 (0.03)	−0.55 (0.52)	−0.29 (0.27)
L	SPT	—	—	—	—	—

(d) Hypothesis 4. Patterns of variation across the SAT, SMT and SPT differ between static and dynamic architecture variables

Within each tufted capuchin, static muscle architecture measurements for the SAT, SMT and SPT were similar (table 3). On average, fibre length was significantly shorter in the SAT than the SMT ($p = 0.02$; electronic supplementary material, figure S3 and table S6), but there were no significant regional differences in pinnation angle (electronic supplementary material, table S6). The SPT had significantly smaller muscle weights and PCSAs compared with the SAT and SMT (all $p < 0.02$; electronic supplementary material, figure S3 and table S6).

In contrast to static muscle architecture, all measures of dynamic muscle architecture showed significant differences

Table 3. Mean static muscle architecture variables for the superficial anterior (SAT), middle (SMT), and posterior (SPT) temporalis for each of the six (three male, three female) adult tufted capuchins. Static measurements were normalized to sarcomere length, bringing estimates to the jaws at or near occlusion [6].

capuchin (sex)	location	sarcomere normalized fibre length (mm)	pinnation angle (°)	physiological cross-sectional area	muscle weight (g)
Se (M)	SAT	14.51	26.44	7.53	12.89
Se (M)	SMT	15.78	27.06	10.89	20.37
Se (M)	SPT	15.69	26.87	4.92	9.14
Mo (M)	SAT	11.05	22.31	5.85	7.38
Mo (M)	SMT	12.08	21.25	5.02	6.88
Mo (M)	SPT	12.05	22.14	2.53	3.48
C2 (M)	SAT	13.85	25.75	5.05	8.20
C2 (M)	SMT	15.39	22.44	7.34	12.92
C2 (M)	SPT	15.05	19.89	3.92	6.63
So (F)	SAT	14.93	23.81	12.01	20.79
So (F)	SMT	15.14	24.05	10.70	18.97
So (F)	SPT	13.99	23.28	5.37	8.65
N (F)	SAT	10.65	18.65	4.35	5.02
N (F)	SMT	11.94	15.12	4.30	5.69
N (F)	SPT	11.78	14.23	2.33	3.19
Ma (F)	SAT	11.34	18.72	3.40	4.27
Ma (F)	SMT	10.78	20.71	3.89	4.75
Ma (F)	SPT	10.45	19.58	3.34	3.91

between regions of the temporalis. Maximum fascicle and muscle lengths were greatest in the SAT followed by the SPT and SMT (all $p < 0.05$; electronic supplementary material, table S7). Minimum coronal fascicle angle was highest in the SAT followed by the SMT and smallest in the SPT, whereas minimum sagittal fascicle angle was highest in the SMT followed by the SAT and smallest in the SPT. By contrast, minimum 3D angle and maximum fascicle and muscle velocities were largest in the SPT and smallest in the SAT or SMT (all $p < 0.05$; electronic supplementary material, table S7). Finally, maximum AGRs were largest in the SMT, followed by the SAT and smallest in the SPT (all $p < 0.05$; electronic supplementary material, table S7).

4. Discussion

Our results suggest that in tufted capuchins regional differences in muscle architecture dynamics primarily reflect the impact of jaw gape, not of muscle activation patterns. On both working and balancing sides gape was the most influential factor driving muscle architecture dynamics in all three regions of the temporalis; relative timing of peaks in muscle architecture dynamics did not match relative timing of peaks in EMG activity across the temporalis. Effects of jaw lateral movements on muscle architecture dynamics were not evident, and there were almost no differences in relative timing of muscle architecture dynamics between working and balancing sides. Fascicle length did reach a minimum significantly later in the balancing SPT than balancing SMT. However, if timing of SPT shortening reflected timing of posterior displacement of the coronoid process, then SPT peak fascicle shortening would occur later on the balancing side than the working side.

It is important to recognize that our static and dynamic muscle architecture data were gathered from a small number of animals, and in one of the females muscle architecture dynamics were only successfully collected from the SAT and SMT. Replication of these results in other taxa and muscles is thus necessary to confidently generalize the results. We also emphasize that our muscle architecture dynamics and EMG data were collected from different animals—precluding definitive intra-individual comparisons of relative timing. However, the relative timing of peak EMG activity in different regions of working and balancing temporalis in our capuchins was similar to that reported for other primates [18]. We note the muscle architecture dynamics data were all from female capuchins whereas the EMG data were mostly from male capuchins. Tufted capuchins have well-documented sexual dimorphism in gape, bite force and diet [89,90], but the influence of sexual dimorphism on the dynamic architecture data presented here is likely to be minimal because the trial foods did not elicit large gapes or high bite forces [90]. Moreover, the effects of jaw gape and movements on muscle architecture dynamics reflect patterns of jaw movement that are also found in other anthropoid primates [17]. Hence, we suspect that our results will be shown to be informative of temporalis muscle architecture dynamics across anthropoids more broadly.

(a) Regional variation in dynamic muscle architecture is driven by gape

Dynamic muscle architecture of the SAT, SMT and SPT was highly correlated with gape across all foods. Fascicle lengths in all three muscle regions were shortest and coronal and sagittal fascicle angles were largest at minimum gape

(figure 2). However, there were regional differences in the relationships between gape and dynamic muscle architecture variables. Comparison of the SPT with the SAT and SMT reveals the slopes of the relationships between gape and fascicle length, muscle length, and 3D fascicle angle were lower, and gape explained less variation in architecture dynamics. The opposite pattern was found for sagittal fascicle angle, and correlations between gape and coronal fascicle angle were similar in the SAT and SPT. As predicted by Iriarte-Diaz *et al.* [17], gape has relatively less impact on muscle architecture dynamics in the SPT than in more anterior portions of the temporalis.

The SAT had longer fascicle and muscle lengths, larger coronal fascicle angles, smaller sagittal and 3D fascicle angles, higher fascicle and muscle velocities, and higher AGRs than the SPT during jaw closing. The presence of anteroposterior variation in superficial temporalis muscle architecture dynamics is consistent with previous studies indicating regional differences in the force output of muscles [28,30]. If the differences in relative timing of temporalis muscle activity in tufted capuchin primates are consistent with other primates, the SAT is involved primarily in jaw elevation whereas the SPT engages in both elevation and jaw retraction [18–20,67,72]. It has been hypothesized that the anterior temporalis is important for bite force-generation across a wide range of feeding behaviours and bite force directions [18,67,69]. In humans variation in bite force direction is associated with less variation in anterior temporalis activity than in other parts of the temporalis [70,91,92]. The human results differ somewhat from electromyography work on the SAT and deep anterior temporalis in baboons. Wall and colleagues [67] observed heavy recruitment of the SAT associated with chewing on hard foods, but the baboons showed low levels of recruitment when feeding on soft foods. Primates likely meet the bite force demands of feeding on mechanically challenging foods in a variety of ways, including (though certainly not limited to) using muscle activation, through variation in activation intensity and differential activation of muscle parts such as the superficial and deep temporalis, and architectural adaptations. While the gross morphology and configuration of the chewing muscles are fairly conserved within and between anthropoid primate taxa (e.g. [54,93]), the arrangement of fibres relative to the force-generating axis of the muscle i.e. pinnation, and the amount of muscle mass allocated to regional parts of the muscles (e.g. superficial versus deep temporalis) vary considerably (e.g. [60,80,94–96]). It thus remains to be tested whether the relative contributions of muscle activation and muscle fibre architecture to bite force vary by taxon.

These findings have implications for tufted capuchin feeding ecology. Tufted capuchins are characterized by feeding on mechanically challenging items, and they have a suite of craniodental features relating to increased bite force production e.g. [80,89]. Behavioural and static architecture data suggest they use large gapes to process and ingest food items [80,89,90,97,98]. Our findings are consistent with static architecture comparisons in tufted capuchins that suggest they are able to feed on large food items that require the generation of relatively wide jaw gapes without compromising bite force [80]. Increased dynamic architectural changes in the SAT, particularly in relation to bite force, would facilitate these performance variables. Dynamic muscle architecture may therefore play an important role in hard object feeding in tufted capuchins.

(b) Food properties and gape are important considerations for modelling the temporalis

Across all foods and gape cycles the temporalis showed very similar dynamic architecture and activation patterns. Overall, the SPT had lower AGR values and greater fascicle shortening relative to the whole muscle, compared with the SAT (electronic supplementary material, table S7), but these muscle regions differed in their associations with mechanically challenging foods. In the SPT our more mechanically challenging foods, i.e. popcorn seeds and unshelled cashews, were associated with higher AGRs compared with marshmallows, red grapes and apple pulp cubes, although we note that ARGs from mechanically challenging foods are limited as SPT data were collected from two of the three animals, and one animal with SPT data would not eat popcorn seeds (figure 3). The opposite pattern was found in the SAT such that mechanically challenging foods were associated with lower AGRs, and the SMT AGRs did not differ with FMPs. While preliminary, these results indicate the SAT likely plays a larger role in FMP-related modulation of bite force compared with the SPT, which is consistent with the SAT's primary role of producing force during jaw elevation compared with the SPT, which produces lower amounts of bite force and both elevates and retracts the jaw [69,70,91,92]. Another possibility is that fibre types differ between these regions, as has been reported for other primates [7], and the SPT operates in a different force/velocity range from the SAT. The SMT was intermediate to the SAT and SPT in most of the dynamic architecture measures and in comparisons between more and less mechanically challenging food groups. While variation in FMPs significantly influenced temporalis muscle architecture dynamics in the anterior and posterior regions, gape dominated dynamic changes in architecture across all foods as well as all muscle regions. The effects of food and gape on architectural dynamics are important considerations for modelling bite forces and loading in primates and other taxa.

Activation of the tufted capuchin temporalis varied anteroposteriorly during the gape cycle such that the working-side SPT was active before the working-side SAT and SMT, and the working-side SPT activated before the balancing-side (electronic supplementary material, figure S1). These results are consistent with previous studies on feeding muscle activation patterns in primates [18–20,67,72]. However, there were few regional differences in dynamic muscle architecture and no consistent pattern was observed (electronic supplementary material, figure S2). This suggests that although regional variation in muscle activation patterns is important for driving anteroposterior and mediolateral translations of the jaw, this regional variation is not associated with regional variation in muscle architecture dynamics. Muscle architecture dynamics instead are largely driven by gape. This finding simplifies modelling of the temporalis in extant and fossil primates in that changes in temporalis architecture can be viewed as a function of gape in relation to bite force production.

(c) Static muscle architecture does not capture regional differences in fibre rotation

Patterns of static and dynamic architecture measurements varied across the temporalis. Static architecture measurements showed limited variation that did not consistently differ across

the regions (electronic supplementary material, figure S3 and table S6). By contrast, there were substantial regional differences in maximum and minimum dynamic muscle architecture variables during jaw closing, with the SAT having consistently higher maximum values in fascicle and muscle length and minimum coronal and sagittal fascicle angle values (electronic supplementary material, figure S3). Some of the difference between patterns of static and dynamic architecture may be related to measurement error [99] as well as the fact that our static measures of temporalis architecture were estimated with the jaws at or very near occlusion (similar to the studies of [100] and [61] for humans and macaques, respectively), while our dynamic estimates for comparison were largely derived from the start of the fast-close phase of the gape cycle (except fascicle and muscle velocity). Nevertheless, the fact that significant regional variation in dynamic architecture of the temporalis is not captured by our static architecture estimates suggests that static architecture likely oversimplifies the complexities of muscle force production and movement capabilities during the gape cycle (see also [6]). Differences in dynamic fascicle angles during jaw closing, as shown in the current study, further underscore the difficulties of accounting for fibre rotation during contractions [4]. While static estimates of jaw-muscle fibre architecture provide reasonable estimates of the maximum force-generating capabilities at a given gape and can be used to estimate and compare isometric bite forces, they are likely unsuitable for modelling the movements and forces over a range of gapes.

Thus, we propose that changes in gape during chewing, rather than muscle recruitment, account for the regional variation we observe in superficial temporalis architecture dynamics in tufted capuchins. These results suggest that models of temporalis force production in extant and extinct primates should take force–gape tradeoffs into account, but that variation in muscle recruitment patterns across the superficial temporalis and between the working and balancing sides may be of less importance, depending on the question. Future work comparing the deep and superficial temporalis, the influence of FMPs, bite force directionality, and sarcomere equivalence in the temporalis will improve our understand of how muscular and neural components interact to produce bite force and jaw movements.

Ethics. All experiments were approved by the University of Chicago IACUC under animal care and use protocols 72430 and 72382.

Data accessibility. The data are provided in the electronic supplementary material [101].

Authors' contributions. M.F.L.: conceptualization, data curation, formal analysis, funding acquisition, investigation, methodology, project administration, writing—original draft, writing—review and editing; J.I.-D.: data curation, formal analysis, methodology, writing—review and editing; C.D.B.: data curation, formal analysis, methodology, writing—review and editing; M.C.G.: data curation, methodology, writing—review and editing; A.B.T.: data curation, formal analysis, methodology, writing—review and editing; C.F.R.: funding acquisition, project administration, resources, supervision, writing—review and editing.

All authors gave final approval for publication and agreed to be held accountable for the work performed herein.

Conflict of interest declaration. We declare we have no competing interests.

Funding. This project was supported by the National Science Foundation (grant nos NSF-BCS-1440516, NSF-BCS-1440541, NSF-BCS-1440542, NSF-BCS-1440545, NSF-BCS-1627206; NSF-BCS-0452160, NSF-BCS-0962677; NSF-BCS-0833394, NSF-BCS-0635649), the National Science Foundation HOMINID (grants nos 0725183 and 0725147), National Institutes of Health (grant no. NIH-R24-HD050837) and the AABA Cobb Award. Funding for the UChicago XROMM Facility was provided by National Science Foundation Major Research Instrumentation (grants nos MRI 1338036 and 1626552). This is University of Chicago XROMM Facility Publication 11.

Acknowledgements. Special thanks to the University of Chicago veterinarians, veterinarian technicians, and animal husbandry staff.

References

1. Gans C. 1965 The functional significance of muscle architecture: a theoretical analysis. *Adv. Anat. Embryol. Cell Biol.* **38**, 115–142.
2. Powell PL, Roy RR, Kanim P, Bello MA, Edgerton VR. 1984 Predictability of skeletal muscle tension from architectural determinations in guinea pig hindlimbs. *J. Appl. Physiol.* **57**, 1715–1721. (doi:10.1152/jappl.1984.57.6.1715)
3. Schumacher G-H. 1961 *Funktionelle morphologie der kaumuskulatur*. Jena, Germany: VEB Gustav Fischer.
4. Lieber RL. 2022 Can we just forget about pennation angle? *J. Biomech.* **132**, 110954. (doi:10.1016/j.jbiomech.2022.110954)
5. Nordstrom SH, Bishop M, Yemm R. 1974 The effect of jaw opening on the sarcomere length of the masseter and temporal muscles of the rat. *Arch. Oral Biol.* **19**, 151–155. (doi:10.1016/0003-9969(74)90209-X)
6. Taylor AB, Terhune CE, Vinyard CJ. 2019 The influence of masseter and temporalis sarcomere length operating ranges as determined by laser diffraction on architectural estimates of muscle force and excursion in macaques (*Macaca fascicularis* and *Macaca mulatta*). *Arch. Oral Biol.* **105**, 35–45. (doi:10.1016/j.archoralbio.2019.05.015)
7. Holmes M, Taylor AB. 2021 The influence of jaw-muscle fibre-type phenotypes on estimating maximum muscle and bite forces in primates. *Interface Focus* **11**, 20210009. (doi:10.1098/rsfs.2021.0009)
8. Korfage JAM, Van Eijden T. 1999 Regional differences in fibre type composition in the human temporalis muscle. *J. Anat.* **194**, 355–362. (doi:10.1046/j.1469-7580.1999.19430355.x)
9. DeMar R, Barghusen HR. 1972 Mechanis and the evolution of the synapsid jaw. *Evolution* **26**, 622–637. (doi:10.1111/j.1558-5646.1972.tb01969.x)
10. Gans C, de Vree F. 1987 Functional bases of fiber length and angulation in muscle. *J. Morphol.* **192**, 63–85. (doi:10.1002/jmor.1051920106)
11. Greaves WS. 1978 The jaw lever system in ungulates: a new model. *J. Zool.* **184**, 271–285. (doi:10.1111/j.1469-7998.1978.tb03282.x)
12. Grossnickle DM. 2017 The evolutionary origin of jaw yaw in mammals. *Scient. Rep.* **7**, 45094. (doi:10.1038/srep45094)
13. Hylander WL, Crompton AW. 1986 Jaw movements and patterns of mandibular bone strain during mastication in the monkey *Macaca fascicularis*. *Arch. Oral Biol.* **31**, 841–848. (doi:10.1016/0003-9969(86)90139-1)
14. Ravosa MJ, Noble VE, Hylander WL, Johnson KR, Kowalski EM. 2000 Masticatory stress, orbital orientation and the evolution of the primate postorbital bar. *J. Hum. Evol.* **38**, 667–693. (doi:10.1006/jhev.1999.0380)
15. Spencer MA. 1999 Constraints on masticatory system evolution in anthropoid primates. *Am. J. Phys. Anthropol.* **108**, 483–506. (doi:10.1002/(SICI)1096-8644(199904)108:4<483::AID-AJPA7>3.0.CO;2-L)
16. Laird MF, Granatosky MC, Taylor AB, Ross CF. 2020 Muscle architecture dynamics modulate performance of the superficial anterior temporalis muscle during chewing in capuchins. *Scient. Rep.* **10**, 6410. (doi:10.1038/s41598-020-63376-y)
17. Iriarte-Diaz J, Terhune CE, Taylor AB, Ross CF. 2017 Functional correlates of the position of the axis of rotation of the mandible during chewing in non-human primates. *Zoology* **124**, 106–118. (doi:10.1016/j.zool.2017.08.006)

18. Hylander WL, Wall CE, Vinyard CJ, Ross C, Ravosa MR, Williams SH. 2005 Temporalis function in anthropoids and strepsirrhines: an EMG study. *Am. J. Phys. Anthropol.* **128**, 35–56. (doi:10.1002/ajpa.20058)
19. Vinyard CJ, Ravosa MJ, Williams SH, Wall CE, Johnson KR, Hylander WL. 2007 Jaw-muscle function and the origin of primates. In *Primate origins: adaptations and evolution* (eds MJ Ravosa, M Dagosto), pp. 179–231. New York, NY: Springer.
20. Vinyard CJ, Wall CE, Williams SH, Hylander WL. 2008 Patterns of variation across primates in jaw-muscle electromyography during mastication. *Integr. Comp. Biol.* **48**, 294–311. (doi:10.1093/icb/icn071)
21. Azizi E, Brainerd EL, Roberts TJ. 2008 Variable gearing in pennate muscles. *Proc. Natl Acad. Sci. USA* **105**, 1745–1750. (doi:10.1073/pnas.0709212105)
22. Brainerd EL, Azizi E. 2005 Muscle fiber angle, segment bulging and architectural gear ratio in segmented musculature. *J. Exp. Biol.* **208**, 3249–3261. (doi:10.1242/jeb.01770)
23. Eng CM, Azizi E, Roberts TJ. 2018 Structural determinants of muscle gearing during dynamic contractions. *Integr. Comp. Biol.* **58**, 207–218. (doi:10.1093/icb/icy054)
24. Holt NC, Danos N, Roberts TJ, Azizi E. 2016 Stuck in gear: age-related loss of variable gearing in skeletal muscle. *J. Exp. Biol.* **219**, 998–1003. (doi:10.1242/jeb.133009)
25. Wakeling JM, Blake OM, Wong I, Rana M, Lee SS. 2011 Movement mechanics as a determinate of muscle structure, recruitment and coordination. *Phil. Trans. R. Soc. B* **366**, 1554–1564. (doi:10.1098/rstb.2010.0294)
26. Camp AL, Astley HC, Horner AM, Roberts TJ, Brainerd EL. 2016 Fluoromicrometry: a method for measuring muscle length dynamics with biplanar videofluoroscopy. *J. Exp. Zool. Ecol. Genet. Physiol.* **325**, 399–408. (doi:10.1002/jez.2031)
27. Rudroff T, Staudenmann D, Enoka RM. 2008 Electromyographic measures of muscle activation and changes in muscle architecture of human elbow flexors during fatiguing contractions. *J. Appl. Physiol.* **104**, 1720–1726. (doi:10.1152/japplphysiol.01058.2007)
28. Azizi E, Deslauriers AR. 2014 Regional heterogeneity in muscle fiber strain: the role of fiber architecture. *Front. Physiol.* **5**, 303. (doi:10.3389/fphys.2014.00303)
29. Cuesta-Vargas AI, Gonzalez-Sanchez M. 2013 Relationship of moderate and low isometric lumbar extension through architectural and muscular activity variables: a cross sectional study. *BMC Med. Imaging* **13**, 38. (doi:10.1186/1471-2342-13-38)
30. Tijs C, Konow N, Biewener AA. 2021 Effect of muscle stimulation intensity on the heterogeneous function of regions within an architecturally complex muscle. *J. Appl. Physiol.* **130**, 941–951. (doi:10.1152/japplphysiol.00514.2020)
31. Anapol F, Herring SW. 1989 Length-tension relationships of masseter and digastric muscles of miniature swine during ontogeny. *J. Exp. Biol.* **143**, 1–16. (doi:10.1242/jeb.143.1.1)
32. Carlson DS. 1977 Condylar translation and the function of the superficial masseter muscle in the rhesus monkey (*M. mulatta*). *Am. J. Biol. Anthropol.* **47**, 53–63. (doi:10.1002/ajpa.1330470111)
33. Carrasco DI, Delp MD, Ray CA. 1999 Effect of concentric and eccentric muscle actions on muscle sympathetic nerve activity. *J. Appl. Physiol.* **86**, 558–563. (doi:10.1152/jappl.1999.86.2.558)
34. Daley MA, Biewener AA. 2003 Muscle force-length dynamics during level versus incline locomotion: a comparison of *in vivo* performance of two guinea fowl ankle extensors. *J. Exp. Biol.* **206**, 2941–2958. (doi:10.1242/jeb.00503)
35. English AW. 1984 An electromyographic analysis of compartments in cat lateral gastrocnemius muscle during unrestrained locomotion. *J. Neurophysiol.* **52**, 114–125. (doi:10.1152/jn.1984.52.1.114)
36. Gabaldón AM, Nelson FE, Roberts TJ. 2004 Mechanical function of two ankle extensors in wild turkeys: shifts from energy production to energy absorption during incline versus decline running. *J. Exp. Biol.* **207**, 2277–2288. (doi:10.1242/jeb.01006)
37. Higham TE, Biewener AA, Wakeling JM. 2008 Functional diversification within and between muscle synergists during locomotion. *Biol. Lett.* **4**, 41–44. (doi:10.1098/rsbl.2007.0472)
38. Hodson-Tole E, Wakeling J. 2007 Variations in motor unit recruitment patterns occur within and between muscles in the running rat (*Rattus norvegicus*). *J. Exp. Biol.* **210**, 2333–2345. (doi:10.1242/jeb.004457)
39. Wang L, Kernell D. 2000 Proximo-distal organization and fibre type regionalization in rat hindlimb muscles. *J. Muscle Res. Cell Motil.* **21**, 587–598. (doi:10.1023/A:1026584307999)
40. Dantuma R, Weijs W. 1980 Functional anatomy of the masticatory apparatus in the rabbit (*Oryctolagus cuniculus* L.). *Neth. J. Zool.* **31**, 99–147. (doi:10.1163/002829680X00212)
41. Turkawski S, Van Eijden T, Weijs W. 1998 Force vectors of single motor units in a multipennate muscle. *J. Dent. Res.* **77**, 1823–1831. (doi:10.1177/00220345980770101001)
42. Turkawski S, Van Eijden T. 2001 Mechanical properties of single motor units in the rabbit masseter muscle as a function of jaw position. *Exp. Brain Res.* **138**, 153–162. (doi:10.1007/s002210100708)
43. Van Ruijven L, Weijs W. 1990 A new model for calculating muscle forces from electromyograms. *Eur. J. Appl. Physiol.* **61**, 479–485. (doi:10.1007/BF00236071)
44. Weijs W, Dantuma R. 1975 Electromyography and mechanics of mastication in the albino rat. *J. Morphol.* **146**, 1–33. (doi:10.1002/jmor.1051460102)
45. Weijs W, Van der Wielen-Drent T. 1982 Sarcomere length and EMG activity in some jaw muscles of the rabbit. *Cells Tissues Organs* **113**, 178–188. (doi:10.1159/000145553)
46. Weijs W, Van der Wielen-Drent T. 1983 The relationship between sarcomere length and activation pattern in the rabbit masseter muscle. *Arch. Oral Biol.* **28**, 307–315. (doi:10.1016/0003-9969(83)90073-0)
47. Gordon A, Huxley AF, Julian F. 1966 The variation in isometric tension with sarcomere length in vertebrate muscle fibres. *J. Physiol.* **184**, 170–192. (doi:10.1113/jphysiol.1966.sp007909)
48. Herring SW, Herring SE. 1974 The superficial masseter and gape in mammals. *Am. Nat.* **108**, 561–576. (doi:10.1086/282934)
49. Hylander WL. 2013 Functional links between canine height and jaw gape in catarrhines with special reference to early hominins. *Am. J. Phys. Anthropol.* **150**, 247–259. (doi:10.1002/ajpa.22195)
50. Porro LB, Holliday CM, Anapol F, Ontiveros LC, Ontiveros LT, Ross CF. 2011 Free body analysis, beam mechanics, and finite element modeling of the mandible of *Alligator mississippiensis*. *J. Morph.* **272**, 910–937. (doi:10.1002/jmor.10957)
51. Ross CF, Iriarte-Diaz J. 2019 Evolution, constraint, and optimality in primate feeding systems. In *Feeding in vertebrates* (ed. VL Bels), pp. 787–829. Berlin, Germany: Springer.
52. Westneat MW. 2003 A biomechanical model for analysis of muscle force, power output and lower jaw motion in fishes. *J. Theor. Biol.* **223**, 269–281. (doi:10.1016/S0022-5193(03)00058-4)
53. Westneat MW. 2004 Evolution of levers and linkages in the feeding mechanisms of fishes. *Integr. Comp. Biol.* **44**, 378–389. (doi:10.1093/icb/44.5.378)
54. Antón SC. 1999 Macaque masseter muscle: internal architecture, fiber length and cross-sectional area. *Int. J. Primatol.* **20**, 441–462. (doi:10.1023/A:1020509006259)
55. Brassard C, Merlin M, Monchâtre-Leroy E, Guintard C, Barrat J, Callou C, Cornette R, Herrel A. 2020 How does masticatory muscle architecture covary with mandibular shape in domestic dogs? *Evol. Biol.* **47**, 133–151. (doi:10.1007/s11692-020-09499-6)
56. Eng C, Ward S, Vinyard C, Taylor A. 2009 The morphology of the masticatory apparatus facilitates muscle force production at wide jaw gapes in tree-gouging common marmosets (*Callithrix jacchus*). *J. Exp. Biol.* **212**, 4040–4055. (doi:10.1242/jeb.029983)
57. Fabre P-H, Herrel A, Fitriana Y, Meslin L, Hautier L. 2017 Masticatory muscle architecture in a water-rat from Australasia (Murinae, *Hydromys*) and its implication for the evolution of carnivory in rodents. *J. Anat.* **231**, 380–397. (doi:10.1111/joa.12639)
58. Herrel A, De Smet A, Aguirre LF, Aerts P. 2008 Morphological and mechanical determinants of bite force in bats: do muscles matter? *J. Exp. Biol.* **211**, 86–91. (doi:10.1242/jeb.012211)
59. Pfaller JB, Gignac PM, Erickson GM. 2011 Ontogenetic changes in jaw-muscle architecture facilitate durophagy in the turtle *Sternotherus minor*. *J. Exp. Biol.* **214**, 1655–1667. (doi:10.1242/jeb.048090)
60. Taylor AB, Vinyard CJ. 2004 Comparative analysis of masseter fiber architecture in tree-gouging

(*Callithrix jacchus*) and nongouging (*Saguinus oedipus*) callitrichids. *J. Morphol.* **261**, 276–285. (doi:10.1002/jmor.10249)

61. Terhune CE, Hylander WL, Vinyard CJ, Taylor AB. 2015 Jaw-muscle architecture and mandibular morphology influence relative maximum jaw gapes in the sexually dimorphic *Macaca fascicularis*. *J. Hum. Evol.* **82**, 145–158. (doi:10.1016/j.jhevol.2015.02.006)
62. Verhulst CD. 2020 3D muscle fiber architecture of avian jaw muscles and their significance for avian cranial functional morphology evolution. *FASEB J.* **34**, 1. (doi:10.1096/fasebj.2020.34.s1.05919)
63. Weijs W, Hillen B. 1985 Cross-sectional areas and estimated intrinsic strength of the human jaw muscles. *Acta Morphol. Neerl. Scand.* **23**, 267–274.
64. Eng CM, Lieberman DE, Zink KD, Peters MA. 2013 Bite force and occlusal stress production in hominin evolution. *Am. J. Phys. Anthropol.* **151**, 544–557. (doi:10.1002/ajpa.22296)
65. Strait DS *et al.* 2009 The feeding biomechanics and dietary ecology of *Australopithecus africanus*. *Proc. Natl Acad. Sci. USA* **106**, 2124–2129. (doi:10.1073/pnas.0808730106)
66. Wroe S, McHenry C, Thomason J. 2005 Bite club: comparative bite force in big biting mammals and the prediction of predatory behaviour in fossil taxa. *Proc. R. Soc. B* **272**, 619–625. (doi:10.1098/rspb.2004.2986)
67. Wall CE, Vinyard CJ, Williams SH, Johnson KR, Hylander WL. 2008 Specialization of the superficial anterior temporalis in baboons for mastication of hard foods. In *Primate craniofacial function and biology* (eds C Vinyard, MJ Ravosa, C Wall), pp. 113–124. Berlin, Germany: Springer.
68. Hylander WL, Johnson KR. 1985 Temporalis and masseter muscle function during incision in macaques and humans. *Int. J. Primatol.* **6**, 289–322. (doi:10.1007/BF02745501)
69. Ross CF, Hylander WL. 2000 Electromyography of the anterior temporalis and masseter muscles of owl monkeys (*Aotus trivirgatus*) and the function of the postorbital septum. *Am. J. Phys. Anthropol.* **112**, 455–468. (doi:10.1002/1096-8644(200008)112:4<455::AID-AJPA4>3.0.CO;2-4)
70. Van Eijden T, Brugman P, Weijs W, Oosting J. 1990 Coactivation of jaw muscles: recruitment order and level as a function of bite force direction and magnitude. *J. Biomech.* **23**, 475–485. (doi:10.1016/0021-9290(90)90303-K)
71. Wall CE, Vinyard CJ, Johnson KR, Williams SH, Hylander WL. 2006 Phase II jaw movements and masseter muscle activity during chewing in *Papio anubis*. *Am. J. Phys. Anthropol.* **129**, 215–224. (doi:10.1002/ajpa.20290)
72. Ram Y, Ross CF. 2018 Evaluating the triplet hypothesis during rhythmic mastication in primates. *J. Exp. Biol.* **221**, jeb165985.
73. Brainerd EL, Baier DB, Gatesy SM, Hedrick TL, Metzger KA, Gilbert SL, Crisco JJ. 2010 X-ray reconstruction of moving morphology (XROMM): precision, accuracy and applications in comparative biomechanics research. *J. Exp. Zool.* **313**, 262–279. (doi:10.1002/jez.589)
74. Eng CM, Roberts TJ. 2018 Aponeurosis influences the relationship between muscle gearing and force. *J. Appl. Physiol.* **125**, 513–519. (doi:10.1152/japplphysiol.00151.2018)
75. Williams SH, Wright BW, den Truong V, Daubert CR, Vinyard CJ. 2005 Mechanical properties of foods used in experimental studies of primate masticatory function. *Am. J. Primatol.* **67**, 329–346. (doi:10.1002/ajp.20189)
76. Signal Developers. 2013 *signal: Signal processing*. See http://r-forge.r-project.org/projects/signal/.
77. Orsbon C, Nakamura Y, Kijak N, Palmer S, Ross C. 2016 Variation in large feeding biomechanics datasets visualized using different dimensionality reduction methods. *Integr. Comp. Biol.* **56**, E345.
78. Söderkvist I, Wedin P-Å. 1993 Determining the movements of the skeleton using well-configured markers. *J. Biomech.* **26**, 1473–1477. (doi:10.1016/0021-9290(93)90098-Y)
79. Anapol F, Shahnoor N, Ross CF. 2008 Scaling of reduced physiologic cross-sectional area in primate muscles of mastication. In *Primate craniofacial function and biology* (eds C Vinyard, MJ Ravosa, C Wall), pp. 201–216. Berlin, Germany: Springer.
80. Taylor AB, Vinyard CJ. 2009 Jaw-muscle fiber architecture in tufted capuchins favors generating relatively large muscle forces without compromising jaw gape. *J. Hum. Evol.* **57**, 710–720. (doi:10.1016/j.jhevol.2009.06.001)
81. Lieber RL, Yeh Y, Baskin RJ. 1984 Sarcomere length determination using laser diffraction. Effect of beam and fiber diameter. *Biophys. J.* **45**, 1007–1016.
82. Walker SM, Schrodt GR. 1974 I segment lengths and thin filament periods in skeletal muscle fibers of the Rhesus monkey and the human. *Anat. Rec.* **178**, 63–81. (doi:10.1002/ar.1091780107)
83. Murphy R, Beardsley AC. 1974 Mechanical properties of the cat soleus muscle in situ. *Am. J. Physiol. Legacy Content* **227**, 1008–1013. (doi:10.1152/ajplegacy.1974.227.5.1008)
84. Byron C, Reed D, Iriarte-Diaz J, Wang Q, Strait D, Laird MF, Ross CF. 2023 Sagittal suture strain in capuchin monkeys (*Sapajus* and *Cebus*) during feeding. *Am. J. Biol. Anthropol.* **180**, 633–654. (doi:10.1002/ajpa.24701)
85. Hylander WL, Ravosa MJ, Ross CF, Wall CE, Johnson KR. 2000 Symphyseal fusion and jaw-adductor muscle force: an EMG study. *Am. J. Phys. Anthropol.* **112**, 469–492. (doi:10.1002/1096-8644(200008)112:4<469::AID-AJPA5>3.0.CO;2-V)
86. R Development Core Team. 2009 *R: a language and environment for statistical computing*. Vienna, Austria: R Foundation for Statistical Computing. See https://www.R-project.org.
87. Barton K. 2009 *MuMIn: multi-model inference*. See http://r-forge.r-project.org/projects/mumin/.
88. Hothorn T, Bretz F, Westfall P. 2008 Simultaneous inference in general parametric models. *Biom. J. Math. Methods Biosci.* **50**, 346–363. (doi:10.1002/bimj.200810425)
89. Wright B. 2005 Craniodental biomechanics and dietary toughness in the genus. *J. Hum. Evol.* **48**, 473–492. (doi:10.1016/j.jhevol.2005.01.006)
90. Laird MF *et al*. 2023 Ontogenetic changes in bite force and gape in tufted capuchins. *J. Exp. Biol.* **226**, jeb245972. (doi:10.1242/jeb.245972)
91. Blanksma N, Van Eijden T. 1990 Electromyographic heterogeneity in the human temporalis muscle. *J. Dent. Res.* **69**, 1686–1690. (doi:10.1177/00220345900690101101)
92. Van Eijden T. 1990 Jaw muscle activity in relation to the direction and point of application of bite force. *J. Dent. Res.* **69**, 901–905. (doi:10.1177/00220345900690031401)
93. Antón SC. 2000 Macaque pterygoid muscles: internal architecture, fiber length, and cross-sectional area. *Int. J. Primatol.* **21**, 131–156. (doi:10.1023/A:1005431831444)
94. Taylor AB, Yuan T, Ross CF, Vinyard CJ. 2015 Jaw-muscle force and excursion scale with negative allometry in platyrrhine primates. *Am. J. Phys. Anthropol.* **158**, 242–256. (doi:10.1002/ajpa.22782)
95. Taylor AB, Terhune CE, Toler M, Holmes M, Ross CF, Vinyard CJ. 2018 Jaw-muscle fiber architecture and leverage in the hard-object feeding sooty mangabey are not structured to facilitate relatively large bite forces compared to other papionins. *Anat. Rec.* **301**, 325–342. (doi:10.1002/ar.23718)
96. Taylor AB, Vinyard CJ. 2013 The relationships among jaw-muscle fiber architecture, jaw morphology, and feeding behavior in extant apes and modern humans. *Am. J. Phys. Anthropol.* **151**, 120–134. (doi:10.1002/ajpa.22260)
97. Norconk MA, Wright BW, Conklin-Brittain NL, Vinyard CJ. 2009 Mechanical and nutritional properties of food as factors in platyrrhine dietary adaptations. In *South American primates: comparative perspectives in the study of behavior, ecology, and conservation* (eds PA Garber, A Estrada, JC Bicca-Marques, EW Heymann, KB Strier), pp. 279–319. Berlin, Germany: Springer.
98. Laird MF *et al.* 2020 Ingestive behaviors in bearded capuchins (*Sapajus libidinosus*). *Scient. Rep.* **10**, 20850. (doi:10.1038/s41598-020-77797-2)
99. Charles J, Kissane R, Hoehfurtner T, Bates KT. 2022 From fibre to function: are we accurately representing muscle architecture and performance? *Biol. Rev.* **97**, 1640–1676. (doi:10.1111/brv.12856)
100. van Eijden TM, Koolstra JH, Brugman P. 1996 Three-dimensional structure of the human temporalis muscle. *Anat. Rec.* **246**, 565–572. (doi:10.1002/(SICI)1097-0185(199612)246:4<565::AID-AR17>3.0.CO;2-M)
101. Laird MF, Iriarte-Diaz J, Byron CD, Granatosky MC, Taylor AB, Ross CF. 2023 Gape drives regional variation in temporalis architectural dynamics in tufted capuchins. Figshare. (doi:10.6084/m9.figshare.c.6836738)